BREAST

Pascal A. T. Baltzer
Anja Schäfer
Matthias Dietzel
David Grässel
Mieczyslaw Gajda
Oumar Camara
Werner A. Kaiser

Diffusion tensor magnetic resonance imaging of the breast: a pilot study

P. A. T. Baltzer (✉) · A. Schäfer ·
M. Dietzel · W. A. Kaiser
Institute of Diagnostic and Interventional
Radiology,
Friedrich Schiller University Jena,
Erlanger Allee 101, 07740, Jena, Germany
e-mail: pascal.baltzer@med.uni-jena.de
Tel.: +49-3641-9324974
Fax: +49-3641-9324832

D. Grässel
Institut für Neurowissenschaften & Medizin
(INM-1),
Forschungszentrum Jülich GmbH, 52425,
Jülich, Germany

M. Gajda
Institute of Pathology,
Friedrich Schiller University Jena,
Ziegmühlenweg 1, 07740, Jena, Germany

O. Camara
Clinic of Gynecology,
Friedrich Schiller University Jena,
Bachstr. 18, 07740, Jena, Germany

Abstract *Objectives* Diffusion-weighted MR imaging has shown diagnostic value for differential diagnosis of breast lesions. Diffusion tensor imaging (DTI) adds information about tissue microstructure by addressing diffusion *direction*. We have examined the diagnostic application of DTI of the breast. *Methods* A total of 59 patients (71 lesions: 54 malignant, 17 benign) successfully underwent prospective echo planar imaging–DTI (EPI-DTI) (1.5T). First, diffusion direction both of parenchyma as well as lesions was assessed on parametric maps. Subsequently, apparent diffusion coefficient (ADC) and fractional anisotropy (FA) values were measured. Statistics included univariate (Mann–Whitney U test, receiver operating analysis) and multivariate (logistic regression analysis, LRA) tests. *Results* Main diffusion direction of parenchyma was anterior–posterior in the majority of cases (66.1%), whereas lesions (benign, malignant) showed no predominant diffusion direction in the majority of cases (23.9%). ADC values showed highest differences between benign and malignant lesions ($P<0.001$) with resulting area under the curve (AUC) of 0.899. FA values were lower in benign (interquartile range, IR, 0.14–0.24) compared to malignant lesions (IR 0.21–0.35, $P<0.002$) with an AUC of 0.751–0.770. Following LRA, FA did not prove to have incremental value for differential diagnosis over ADC values. *Conclusions* Microanatomical differences between benign and malignant breast lesions as well as breast parenchyma can be visualized by using DTI.

Keywords Breast MRI · Diffusion tensor MRI · MR mammography · Sensitivity and specificity

Introduction

Breast MRI is the most sensitive method for the detection of breast cancer [1, 2]. The basic breast MRI protocol includes intravenous injection of a contrast agent followed by repetitive T1w image series [3, 4]. This approach visualizes the vasculature of malignant neoplasms. As angiogenesis of malignant lesions is induced at an early stage of disease, breast cancer might be detected at sizes above 2–3 mm [3, 5]. However, hypervascularization is also frequently observed in benign lesions. This is why specificity of enhancement pattern analysis in breast MRI sometimes is not sufficient for differential diagnosis as a standalone method [6–8]. Consequently, more sophisticated methods for enhancement pattern analysis such as computer-assisted evaluation or pharmacokinetic modeling, as well as analysis of morphologic lesion profiles, have been suggested [9, 10]. The MRI Breast Imaging-Reporting and Data System (BI-RADS) lexicon recommends combination of dynamic and morphological criteria for differential diagnosis of breast lesions [11].

Besides morphologic criteria, the search for specific predictors of malignant breast disease includes new techniques like MR spectroscopy or diffusion-weighted imaging (DWI) [12–15]. The latter is able to visualize and quantify the random Brownian motion of molecules in vivo. As quantitative diffusivity—described by the apparent diffusion coefficient (ADC)—is influenced by tissue microstructure (e.g., extracellular space fraction, tissue cellularity), the approach behind this method is different and—possibly—complementary to contrast-enhanced breast MRI. The inherent advantages of DWI include fast image acquisition by the echo planar imaging (EPI) technique along with the avoidance of contrast agent injection providing quantitative data comparable between different sequences, MR systems, and field strengths [15]. Previous investigations consistently report a high diagnostic reliability of this method for differentiation of breast lesions [16–30]. The basic technical concept of DWI is to insert two diffusion-sensitizing field gradients into a pulse sequence, compensating for each other and therefore preserving the signal in case of stationary spins. By contrast, incoherent motion (i.e., diffusion) leads to incomplete spin rephasing and therefore to a diffusion-dependent signal loss [31]. If at least six gradient directions are applied, a symmetrical matrix, the diffusion tensor, can be calculated, describing the anisotropic water diffusion in the tissue. It can be visualized by using an ellipsoid, characterized by three eigenvalues representing their respective diffusivities (the length of the principal axes of the ellipsoid) and their corresponding directions (eigenvectors). The sum of the eigenvalues gives the diffusion trace. The proportion of the eigenvectors characterizes the diffusion isotropy. Isotropic diffusion (e.g., in large compartments) is characterized by equal eigenvalues and can be visualized by using a sphere, whereas a high degree of tissue structuring causes anisotropic diffusion represented by a prolate or oblate ellipsoid (e.g., in the white matter of the brain) [32]. As the breast is a structured organ, presenting with fibroglandular tissue orientated along tubular ducts and Cooper ligaments, the hypothesis of this study was that changes of this tissue structure by means of benign or malignant tumor growth would be reflected by changes in diffusion anisotropy. Consequently, this investigation aimed to identify possible differences of breast neoplasms and parenchyma regarding diffusion anisotropy. Furthermore, the possible diagnostic value of diffusion tensor imaging (DTI) for detection and differential diagnosis of breast lesions was examined.

Materials and methods

Patient population and standard of reference

All 635 female patients referred to MR mammography in our department by the local clinic of gynecology between 12 March 2007 and 21 April 2008 were eligible for this prospective investigation which had ethics review board approval. Reasons for referral were unclear or suspicious findings in x-ray mammography, ultrasound of the breast, or by means of clinical examination. Out of these, a total of 67 patients (mean age 54.6 years, standard deviation 15.7 years) satisfied the inclusion criterion: enhancing lesions larger than 5 mm in diameter detected by contrast-enhanced MR mammography. These patients were randomly chosen to additionally undergo unilateral diffusion tensor imaging of the lesion-bearing breast in the same session. Randomization was dependent on seasonal, non-systematic magnet time confinements and eligible patients were chosen before the examination. In cases without enhancing lesions, DTI was not performed. To the best of our knowledge, there was no connection between special indications/cases and examination scheduling. Standard of reference for MRI results was either histopathology performed by a board certified breast pathologist (M.G.) or clinical and radiological follow-up. Exclusion criteria were previous surgery, radiation or chemotherapy of breast cancer, incomplete examination or non-diagnosable images, i.e., due to artifacts. This prospective investigation was approved by the local ethics committee, and all patients gave their written informed consent for the examination.

Routine MR imaging

All examinations were performed on the same 1.5-T clinical whole body MRI system (Magnetom Sonata, Siemens Healthcare, Erlangen, Germany) using a dedicated receive-only bilateral breast coil (CP Breast Array Coil, Siemens Healthcare, Erlangen, Germany) consisting of 4 coil elements with 4 integrated preamplifiers. All MR imaging was performed with the patient in prone position. The routine imaging protocol consisted of a dynamic axial T1-weighted gradient echo sequence (FLASH 2D, GRAPPA factor 2, repetition time (TR) 113 ms, echo time (TE) 5 ms, flip angle 80°, spatial resolution $1.1 \times 0.9 \times 3$ mm, acquisition time 1 min per measurement). After the first measurement, intravenous bolus injection of 0.1 mmol/kg body weight gadopentetate dimeglumine (Gd-DTPA, Magnevist, Bayer HealthCare, Leverkusen, Germany) at 3 ml/s by an automatic injector (Spectris, Medrad, Pittsburgh, USA) was performed, followed immediately by 20 ml of a saline solution. Thirty seconds after contrast agent injection, dynamic MR imaging was continued, using the same sequence parameters and tuning conditions, for a total of 7 contrast-enhanced measurements. Routine MR imaging was completed by axial T2-weighted turbo-spin-echo images (T2w-TSE, GRAPPA factor 2, TR 8,900 ms, TE_{eff} 207 ms, flip angle 90°, spatial resolution $0.8 \times 0.7 \times 3$ mm, acquisition time 2 min 15 s) as well as images from an axial turbo spin echo inversion recovery sequence with magnitude

reconstruction (TIRM, GRAPPA factor 2, TR 8,420 ms, TE_{eff} 70 ms, TI 150 ms, flip angle 180°, spatial resolution $1.7 \times 1.4 \times 3$ mm, acquisition time 2 min 33 s) in identical slice positions.

MR diffusion tensor imaging and postprocessing

After manual shimming and frequency adjustments, diffusion tensor imaging was performed by using unilateral acquisition of an echo planar imaging sequence in coronal orientation (EPI-DTI, TR 8,800 ms, TE_{eff} 139 ms, voxel size $1.5 \times 1.5 \times 5$ mm, no distance factor, 40 slices, bandwidth 1,346 Hz, 6/8 partial Fourier, no parallel imaging, spectral fat saturation, echo distance 0.86 ms, EPI factor 128, 6 diffusion directions, 2 diffusion weightings $b0$ and $b1,000$ s/mm^2, 5 averages, acquisition time 5 min 17 s).

Diffusion tensor data were postprocessed on the MRI console using the Neuro3D toolbox (Siemens Healthcare, Erlangen, Germany) applying a $b0$ threshold of 50 AU. Eigenvalues (diffusivities) λ_1, λ_2, and λ_3 as well as eigenvectors $\mathbf{v}_1$, $\mathbf{v}_2$, and $\mathbf{v}_3$ are automatically determined in each voxel. Mean diffusivity (MD), referred to as apparent diffusion coefficient (ADC) and expressed in 10^{-3} mm^2/s was calculated according to Eq. 1 from the diffusion trace.

$$MD = \lambda_m = \frac{(\lambda_1 + \lambda_2 + \lambda_3)}{3} \tag{1}$$

Fractional anisotropy (FA) describes diffusion anisotropy quantitatively on a range from 1 (maximum anisotropy) to 0 (isotropic diffusion). It was calculated according to Eq. 2.

$$FA = \sqrt{\frac{3}{2}} \cdot \frac{\sqrt{(\lambda_1 - \lambda_m)^2 + (\lambda_2 - \lambda_m)^2 + (\lambda_3 - \lambda_m)^2}}{\sqrt{\lambda_1^2 + \lambda_2^2 + \lambda_3^2}} \tag{2}$$

FA could be displayed as a grayscale map or colored map with color-coding of main tensor direction in the x-, y-, or z-axis (i.e., anterior–posterior, left–right, or cranial–caudal). Examples of DTI images and parametric maps are shown together with anatomical images in Figs. 1, 2, and 3.
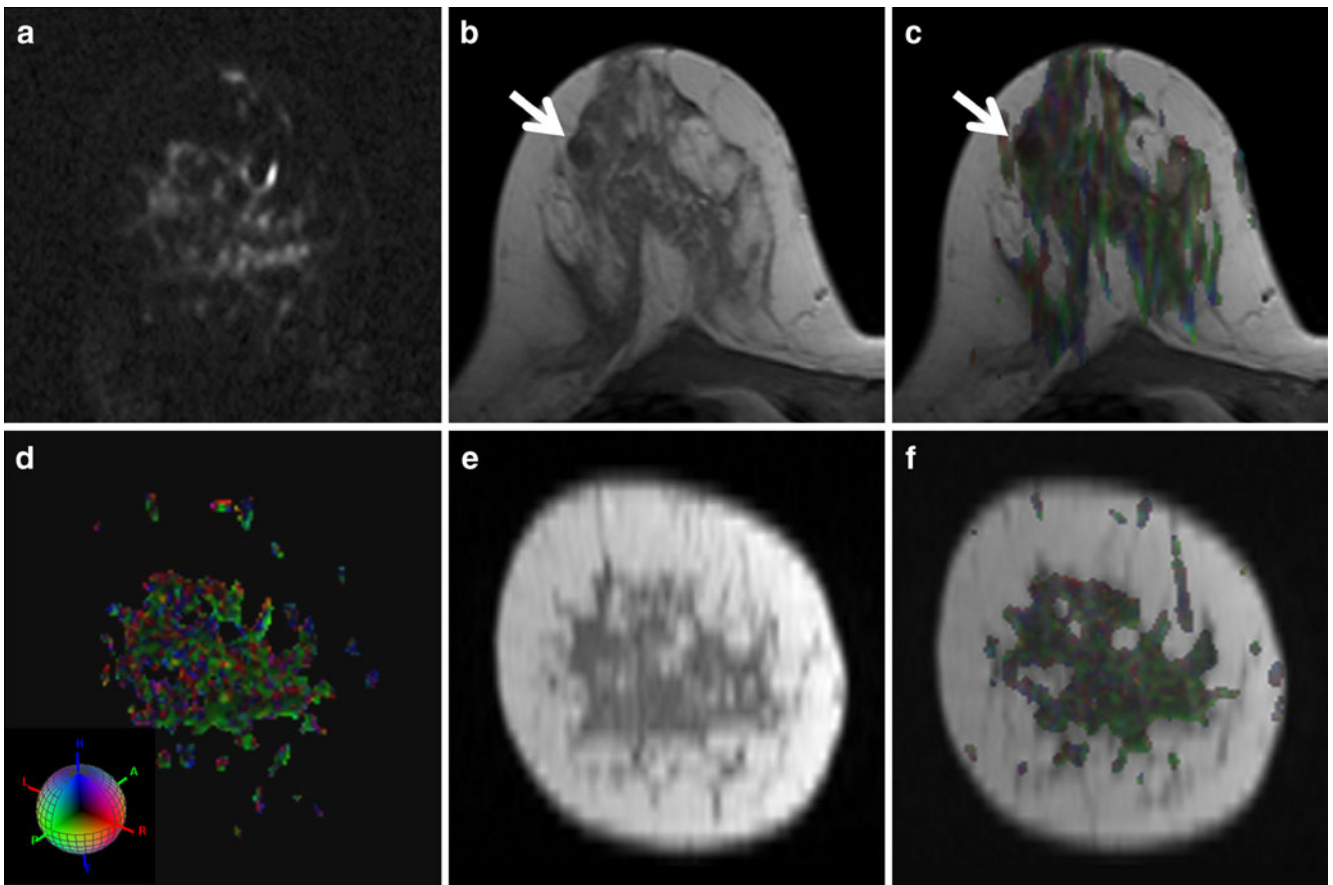

Fig. 1 Example of DTI fusion in a 46-year-old patient. *A* $b1,000$ s/mm^2 diffusion-weighted image, *D* fractional anisotropy (FA) map with voxelwise color-coding of main diffusion direction. *Brightness* codes the degree of anisotropy according to given scales between 0 and 1. *B* anatomical T1w gradient echo image with coronal reconstruction (*E*) showing isointense parenchyma and hyperintense fatty tissue. *C, F* registered anatomical and DTI images. Besides some artifacts, main voxel color is *green* (anterior–posterior diffusion), reflecting ductal orientation. Furthermore, green voxels are brighter compared to most *blue* and *red* voxels (higher FA). Note markedly reduced FA in a lateral cyst (*arrow*)
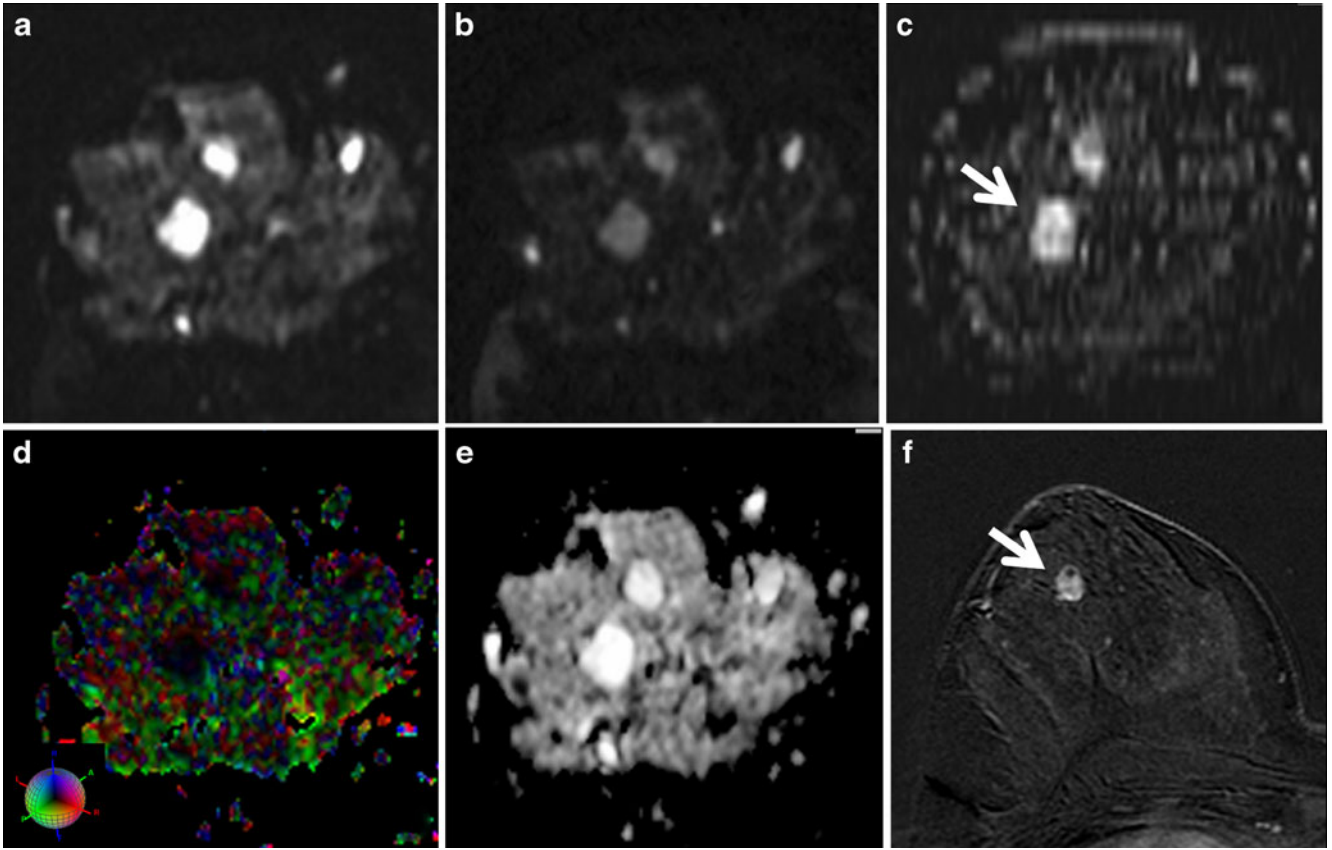
Fig. 2 A 50-year-old female showing a lobulated mass with inhomogeneous internal enhancement and cystic component (*arrow*) on early contrast-enhanced T1w subtraction image (*F, C* coronal reconstruction). *A* $b0$ s/mm^2 image, showing lobulated mass with high signal intensity. *B* $b1,000$ s/mm^2 image demonstrates a distinct signal loss, the corresponding ADC map (*E*) shows high signal intensity. Color-coded FA map demonstrates very low anisotropy (hypointensity) inside the lesion without predominant diffusion direction. These findings are typical for fibroadenoma, which was verified by histopathology. Note the second similar lesion at 12:00

Data analysis

All imaging data were prospectively analyzed by an experienced radiologist (P.A.T.B., 5 years' experience of MR mammography, 2 years' experience of breast DWI) using the Viewer and Neuro3D toolbox (Siemens Healthcare, Erlangen, Germany). After determination of the lesion's maximum diameter on the first contrast-enhanced subtraction images, these were co-registered with diffusion-weighted trace images (averaged diffusion-weighted images at $b=1,000$ s/mm^2, cf. Fig. 1). Subsequently, four regions of interest (ROI) were drawn. The first ROI (ROI$_{lesion}$) encircled the complete lesion on diffusion-weighted images on the slice showing maximum lesion diameter, omitting non-vital zones (i.e., slow- or non-enhancing lesion parts) in order to avoid partial volume effects. The second, smaller ROI (ROI$_{peak}$) was placed in the brightest part of the analyzed lesion on diffusion-weighted trace images, omitting regions with very high T2w signal intensity (i.e., cysts, necrosis). Considering T2w ($b0$) images, the third ROI (ROI$_{parenchyma}$) was placed in a representative large part of fibroglandular tissue macroscopically unaffected by the pathological lesion, avoiding selective measurement of cysts or liquid filled ducts. The last ROI (ROI$_{noise}$) was placed in the noise outside the breast. All regions of interest were automatically transferred to the parametric ADC and FA maps as well as the T1w contrast-enhanced subtraction image. If a misregistration between DWI and T1w subtraction images occurred, the first three ROI were placed anew on subtraction images.

In order to compare lesion contrast between both methods, contrast to noise ratios (CNR) for diffusion-weighted trace images ($b=1,000$ s/mm^2) as well as T1w contrast-enhanced subtraction images were calculated from the mean grayvalues of ROI$_{lesion}$, ROI$_{parenchyma}$ as well as ROI$_{noise}$ according to Eq. 3.

$$CNR = \frac{(ROI_{lesion} - ROI_{parenchyma})}{ROI_{noise}} \qquad (3)$$

Before ROI analysis, the radiologist visually assessed color-coded FA maps for predominant color in fibroglandular tissue as well as enhancing lesions. After the visual
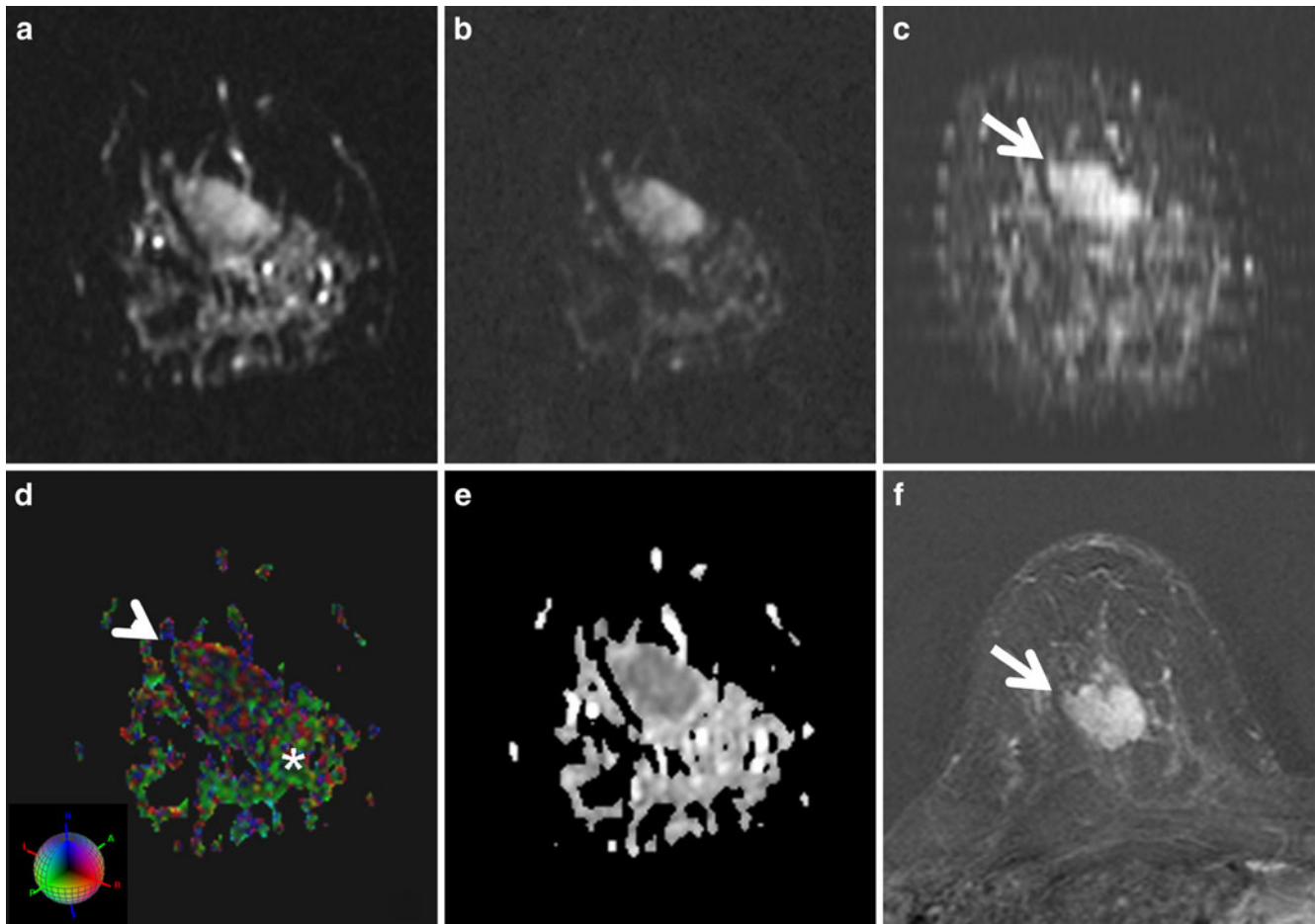
Fig. 3 A 46-year-old female showing an ill-defined mass lesion with inhomogeneous internal enhancement (*arrow*) on early contrast-enhanced T1w subtraction image (*F, C* coronal reconstruction). *A, B* Comparing $b0$ s/mm^2 with the $b1{,}000$ s/mm^2 image, diffusion-dependent signal loss of fibroglandular tissue is stronger than that of the lesion. Accordingly, the corresponding ADC map (*E*) shows low signal intensity. Color-coded FA map shows the lesion (*arrowhead*) a little more hypointense compared to breast tissue (*asterisk*), the lesion does not have a predominant diffusion direction. These findings are typical for invasive breast cancer, which was verified by histopathology (invasive ductal cancer, G2)

Table 1 Characteristics and reference standard of malignant lesions

		Number (n)
BI-RADS type	Mass	48
	Non-mass	6
Reference standard	Core biopsy	12
	Breast conservative surgery	22
	Mastectomy	20
	Follow-up ≥12 months[b]	1
Subgroups	Invasive ductal	37
	Invasive lobular	2
	Invasive ductal and lobular	7
	Other	7
Grading[a]	DCIS	1
	G1	2
	G2	17
	G3	31
Size	Median; 25th–75th percentile	21.5; 15–39.25

DCIS ductal carcinoma in situ

[a] Four gradings including DCIS and leukaemia case not obtained

[b] Leukemic infiltration

assessment, color ratings were compared with direction encoding, which was not known at the time of rating. Diffusivity could either show no predominant direction or predominant direction in the x-, y-, or z-axis.

Statistics

Group comparisons of scaled values were performed by using the Mann–Whitney U test. The Wilcoxon signed rank test was applied for intraindividual comparisons. Visual predominant diffusion direction assessment was compared between lesions and parenchyma using the chi-square test for independent samples. ADC and FA values were further analyzed by receiver operating characteristics (ROC).

In order to identify independent predictors for tumor type (i.e., benign vs. malignant), binary logistic regression analysis was performed. Covariates used were ADC and FA values obtained from ROI$_{lesion}$ and

Table 2 Characteristics and reference standard of benign lesions

		Number (*n*)
BI-RADS type	Mass	17
	Non-mass	0
Reference standard	Core biopsy	10
	Open surgery	4
	Follow-up ≥12 months[a]	2
Subgroups	Fibroadenoma	13
	Papilloma	1
	Fibrocystic disease	2
	Abscess	1
Size (mm)	Median; 25th–75th percentile	12; 15–21.5

[a] Two known fibroadenomas

ROI$_{peak}$ as well as the maximum diameter of the lesion to account for possible size-dependent differences. Stepwise backward feature selection based on likelihood ratios was used with 0.05 and 0.1 as enter and remove limit for covariate probabilities until only independent features were left. All tests in this study were performed two-sided, and α was set to 5%. The statistic used in this paper has exploratory character.

Results

Patients and lesions

Out of 67 patients investigated, 8 had to be excluded because of susceptibility artifacts after previous vacuum biopsy (*n*=4), inconsistent DTI data (*n*=3), or failed fat saturation due to wrong frequency adjustments (*n*=1). Thus, 59 patients remained. Indications for breast MRI were as follows: 18 with biopsy proven breast cancer (30.5%), 25 with suspicious lesions in x-ray mammography or ultrasound (42.4%), one with unclear conventional findings, two for cancer screening (3.4%), five with clinical findings only (8.5%; i.e., nipple discharge, inflammation), and eight with follow-up of probably benign lesions. These patients showed 71 lesions in contrast-enhanced MR mammography; details are given in Tables 1 and 2.

CNR comparison between diffusion-weighted and contrast-enhanced T1w subtraction images

CNR values of lesions on diffusion-weighted images (mean 34.8, SD 52.8) were not significantly (*P*=0.191) lower compared to those of T1w subtraction images (mean 32.1, SD 21.4).

Comparing benign with malignant CNR values, both diffusion-weighted and contrast-enhanced T1w subtraction images of benign lesions (DWI: mean 22.1, SD 13.6; subtraction: mean 22.2, SD 13.3) showed significantly lower values (*P*=0.050 DWI, *P*=0.005 subtraction) compared with malignant lesions (DWI: mean 31.4, SD 26.3; subtraction: mean 37.2, SD 32.1).

ADC values (cf. Table 3, Fig. 4)

ADC values obtained from ROI$_{lesion}$ and ROI$_{peak}$ in benign lesions were significantly higher than in malignant lesions (*P*<0.001). Case by case comparison showed that ADC$_{peak}$ values were significantly lower than ADC$_{lesion}$ values in malignant (*P*=0.001), but not in benign lesions (*P*=0.588). ADC$_{lesion}$ values of benign lesions did not differ significantly from ADC$_{parenchyma}$ in benign lesions (*P*=0.089). However, significant differences between ADC$_{lesion}$ and ADC$_{parenchyma}$ were found in malignant lesions (*P*<0.001). ADC$_{peak}$ was significantly higher compared to ADC$_{parenchyma}$ in benign (*P*=0.045) and significantly lower than ADC$_{parenchyma}$ in malignant lesions (*P*<0.001). Examples of ADC in benign and malignant lesions are shown in Figs. 2 and 3, respectively.

FA values (cf. Table 3, Fig. 5)

FA was significantly lower in benign compared to malignant lesions with *P* values of 0.001 (FA$_{lesion}$) and 0.002 (FA$_{peak}$). FA$_{peak}$ values were significantly lower both in benign and malignant lesions compared to FA$_{lesion}$ values (*P*=0.039 and *P*<0.001). FA$_{parenchyma}$ values did not differ significantly from FA$_{lesion}$ values in malignant lesions (*P*=0.839), whereas FA$_{lesion}$ values in benign lesions were significantly lower than FA$_{parenchyma}$ values (*P*=0.003). Regarding FA$_{peak}$ values, these were signifi-

Table 3 ADC and FA values obtained from ROI$_{lesion}$, ROI$_{peak}$, and ROI$_{parenchyma}$ with corresponding *P* values for group comparisons between benign and malignant lesions

Tissue	Benign		Malignant		*P* value
	Median	25th–75th percentile	Median	25th–75th percentile	
ADC$_{lesion}$	1.62	1.39–1.77	0.87	0.79–1.07	<0.001
ADC$_{peak}$	1.6	1.48–1.83	0.8	0.69–0.95	<0.001
ADC$_{parenchyma}$	1.29	0.89–1.61	1.16	0.86–1.67	0.811
FA$_{lesion}$	0.18	0.14–0.24	0.26	0.21–0.35	0.001
FA$_{peak}$	0.15	0.11–0.18	0.21	0.16–0.29	0.002
FA$_{parenchyma}$	0.23	0.20–0.36	0.27	0.22–0.41	0.379

ADC values are given in $\times 10^{-3}$ mm^2/s; FA values can range from 0 to 1

cantly lower in benign lesions ($P=0.001$) as well as in malignant lesions ($P=0.041$) compared to $FA_{parenchyma}$. Examples of FA in parenchyma, benign, and malignant lesions are shown in Figs. 1, 2, and 3, respectively.

Visual diffusion direction

Thirteen out of 54 malignant lesions (24.1%) showed a predominant diffusion direction, 10 out of them in the anterior–posterior (x-axis) direction (nine invasive carcinoma, one DCIS). Four out of 17 benign lesions (23.5%; two papilloma, two fibroadenoma) showed a predominant diffusion direction (one in the x-, two in y-, and one in the z-axis). On the contrary, in 43 out of 59 (72.9%) patients, a predominant diffusion direction of fibroglandular tissue could be visualized, 39 out of them demonstrating anisotropic diffusion in the anterior–posterior direction (66.1%). The difference between lesions and fibroglandular tissue was of statistical significance ($P<0.001$).

ROC and binary LRA (cf. Table 4, Fig. 6)

Area under the curve (AUC) was found between 0.894 and 0.899 for ADC values without significant differences between ADC_{lesion} and ADC_{peak} measurements ($P=0.792$).

Regarding FA values, AUC ranged from 0.751–0.770 without significant differences between FA_{lesion} and FA_{peak} ($P=0.688$).
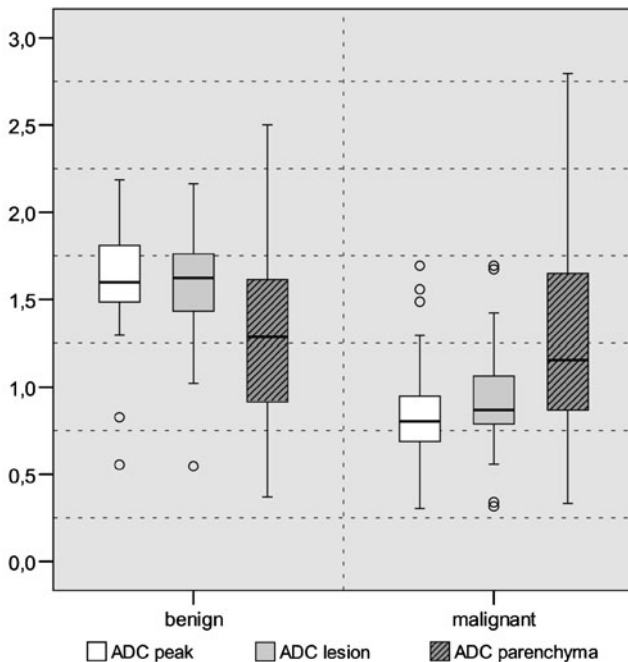

Fig. 5 FA measurement results obtained from ROI_{peak}, ROI_{lesion}, and $ROI_{parenchyma}$ as boxplots clustered by lesion type (benign vs. malignant)
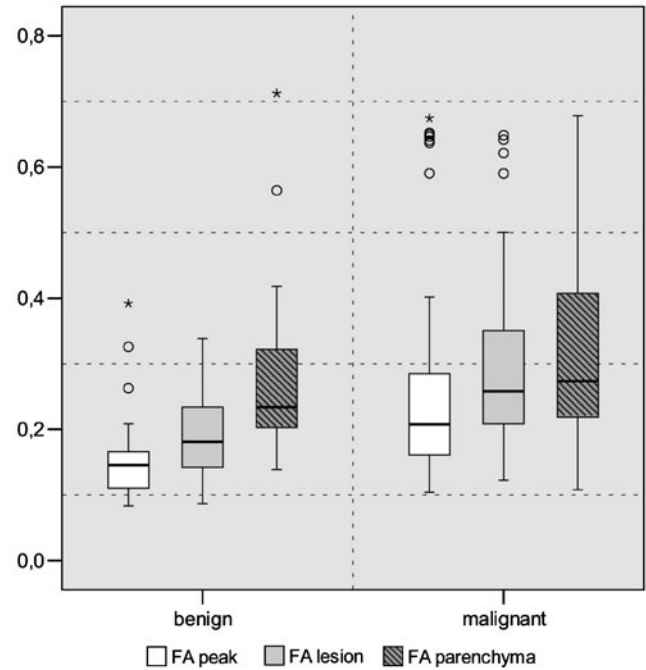
Only ADC_{peak} was retained by logistic regression analysis ($P=0.001$) at an overall Nagelkerke's R^2 of 0.616.

Discussion

Diffusion-weighted imaging (DWI) of the breast is increasingly used for breast lesion differentiation. ADC values have been consistently described as being high in benign and low in malignant lesions [18–30]. A recent meta-analysis reports pooled sensitivity and specificity values of 89% and 77%, respectively [15]. However, there are pathological entities which do not match the described characteristics of benign and malignant lesions because of overlapping ADC values [17]. This explains the need to improve diagnostic accuracy of DWI. In this study, we were able to show the feasibility of diffusion tensor imaging for differential diagnosis of breast lesions. Contrast to noise ratio (CNR) of early T1w subtraction images did not differ significantly from diffusion-weighted trace images. As CNR is an objective measurement of lesion contrast, this finding underlines the possibility to detect breast lesions by DWI. Besides mean diffusivity (ADC) values, fractional anisotropy (FA) also differed between benign and malignant findings. FA values of parenchyma were higher than those of benign lesions but at the same level as those of malignant lesions. This is of interest, since ADC values are claimed to represent tissue cellularity or extracellular space fraction, whereas FA values are thought to reflect tissue structuring.

Fig. 4 ADC measurement results obtained from ROI_{peak}, ROI_{lesion}, and $ROI_{parenchyma}$ as boxplots clustered by lesion type (benign vs. malignant)

Table 4 Receiver operating characteristics analysis of ADC and FA values with resulting sensitivity and specificity values

	AUC	SE	P value	Sensitivity[a]	Specificity[a]	Cutoff
ADC$_{lesion}$	0.894	0.059	0.0001	87.0% (95% CI 75.1–94.6)	88.2% (95% CI 63.6–98.5)	≤1.16[b]
ADC$_{peak}$	0.899	0.059	0.0001	92.6% (95% CI 82.1–97.9)	88.2% (95% CI 63.6–98.5)	≤1.29[b]
FA$_{lesion}$	0.770	0.067	0.0001	79.6% (95% CI 66.5–89.4)	64.7% (95% CI 38.3–85.5)	>0.194
FA$_{peak}$	0.751	0.076	0.001	72.2% (95% CI 58.4–83.5)	76.5% (95% CI 50.1–93.2)	>0.166

AUC area under the curve, *SE* standard error

[a] Applying cutoff value

[b] $\times 10^{-3}$ mm^2/s

The latter was more decreased in benign lesions compared to malignant lesions and macroscopically healthy breast tissue. Furthermore, the majority of lesions showed no predominant diffusion direction by visual inspection, whereas unaffected fibroglandular tissue showed a dominant diffusion direction in anterior–posterior direction (i. e., the direction of the majority of glandular ducts toward the nipple) in a large fraction of patients (66.1%).

According to our hypothesis based on histopathological knowledge, most breast pathologies result in decreased structuring compared to healthy tissue. Therefore, reduced diffusion anisotropy was expected. According to our results, this hypothesis could be confirmed. An exclusion criterion of our study was cancer surgery before the examination. Post-surgical changes distort tissue anatomy and would likely be reflected by a reduced diffusion anisotropy. In such a situation, the value of DTI in differentiating tissue types might be limited. Two recent investigations by the same group reported on FA values in unaffected and malignant breast tissue [33, 34]. Their

Fig. 6 ROC curves of ADC$_{peak}$ and FA$_{peak}$ values. As corresponding ROC curves obtained from ROI$_{lesion}$ measurements did not differ significantly from ROI$_{peak}$ measurements, these data are not displayed

results regarding FA values of malignant lesions as well as unaffected breast parenchyma are in congruence with our results; however, they reported somewhat higher FA values in benign lesions (mean 0.24±0.08 compared to mean 0.19±0.07 in our study; difference is −0.05, 95% CI −0.097 to −0.003). As the proportion of non-mass-like enhancements and foci in the cited investigation was especially high in the benign subgroup (55%), we explain these differences by partial volume effects due to a limited spatial resolution of the DTI technique used (1.9×1.9× 5 mm). Consequently, higher FA values in benign lesions reduce the FA difference between benign and malignant lesions and thus the diagnostic value for lesion discrimination in ROC analysis. This explains why Partridge et al. could not demonstrate a diagnostic value for breast lesion differentiation using FA values. However, this limitation also holds true for the DTI technique used in our study and further investigation on improved DTI technique and on representative numbers in lesion subgroups is warranted to clarify this matter.

Further limitations of the present study have to be discussed. Although the DTI technique used provides a high signal to noise ratio (SNR), small and subtle foci might be missed because of partial volume effects. The echo planar imaging (EPI) technique used in this study provides the highest SNR for diffusion-weighted imaging of the breast, but, on the other hand, is susceptible to coherent motion of lungs and heart as well as gross patient movement [18, 31]. Furthermore, fat saturation is mandatory using the EPI technique and incomplete fat saturation can be another possibility of technical failure [16]. Another limitation of the present study we are obliged to mention is the patient collective. As only patients with enhancing lesions (lesions being defined according to BI-RADS) were chosen for DTI and the common fibrocystic disease most often represents as foci or bilateral background enhancement, benign lesions in the present study mainly represent solid tumors, i.e., fibroadenoma. Fibroadenomas are the most frequent benign tumors of the breast, characterized by distinct histopathological features which are a fibroid stroma together with glandular structures. Here, high ADC and low FA values are to be expected, because elevated myxoid extracellular matrix and absence of oriented tubular structures are characteristic features of fibroadenoma. Following lesion composition in the present investigation, results may not be applied to a screening
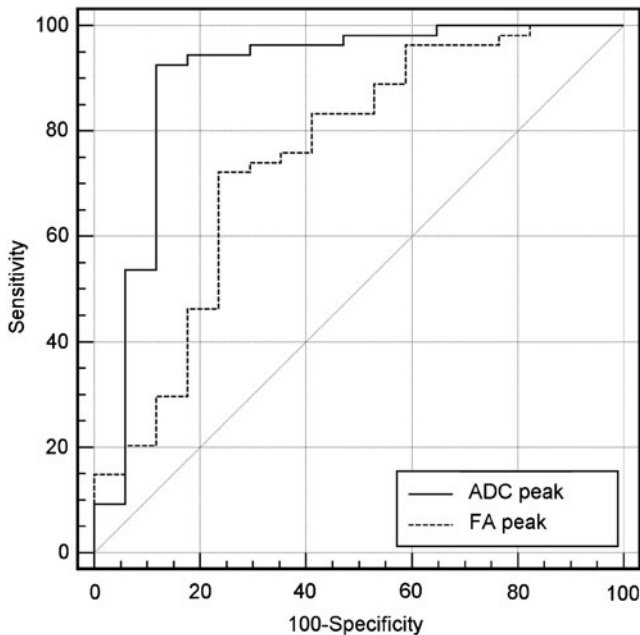
setting, where masses are thought to be absent and the imaging technique applied has to detect and differentiate subtle, non-mass-like stages of breast disease. As has been stated above, the use of DTI in this setting is of interest. In this study, according to LRA, FA did not prove to have incremental value compared to ADC values; Partridge et al., investigating a high proportion of non-mass-like enhancements, could not differentiate between malignant and benign lesions by FA measurements [34]. We hypothesize that a DTI technique with an improved spatial resolution might be of additional value for differential diagnosis addressing diffusion direction. Consequently,

further investigation on this matter, preferably with detailed histopathological backup, is necessary.

In conclusion, we have demonstrated the feasibility of DTI of the breast. Not only mean diffusivity but also diffusion anisotropy significantly differs between different breast neoplasms. CNR of breast lesions on DWI is high enough and not significantly inferior to that of T1w contrast-enhanced subtraction images. These particulars might be used for semiautomatic detection and quantitative assessment of breast lesions. However, in the presented setting, FA values did not show an incremental diagnostic value compared to ADC measurements only.

References

1. Peters NH, Borel Rinkes IH, Zuithoff NP et al (2008) Meta-analysis of MR imaging in the diagnosis of breast lesions. Radiology 246:116–124
2. Warner E, Messersmith H, Causer P et al (2008) Systematic review: using magnetic resonance imaging to screen women at high risk for breast cancer. Ann Intern Med 148:671–679
3. Kaiser WA, Zeitler E (1989) MR imaging of the breast: fast imaging sequences with and without Gd-DTPA. Preliminary observations. Radiology 170:681–686
4. Kuhl C (2007) The current status of breast MR imaging. Part I. Choice of technique, image interpretation, diagnostic accuracy, and transfer to clinical practice. Radiology 244:356–378
5. Naumov GN, Bender E, Zurakowski D et al (2006) A model of human tumor dormancy: an angiogenic switch from the nonangiogenic phenotype. J Natl Cancer Inst 98:316–325
6. Baltzer PA, Freiberg C, Beger S et al (2009) Clinical MR-mammography: are computer-assisted methods superior to visual or manual measurements for curve type analysis? A systematic approach. Acad Radiol 16:1070–1076
7. Gibbs P, Liney GP, Lowry M et al (2004) Differentiation of benign and malignant sub-1cm breast lesions using dynamic contrast enhanced MRI. Breast 13:115–121
8. Siegmann KC, Muller-Schimpfle M, Schick F et al (2002) MR imaging-detected breast lesions: histopathologic correlation of lesion characteristics and signal intensity data. AJR Am J Roentgenol 178:1403–1409
9. Zwick S, Brix G, Tofts PS et al (2009) Simulation-based comparison of two approaches frequently used for dynamic contrast-enhanced MRI. Eur Radiol 20:432–442
10. Tofts PS, Berkowitz B, Schnall MD (1995) Quantitative analysis of dynamic Gd-DTPA enhancement in breast tumors using a permeability model. Magn Reson Med 33:564–568
11. Ikeda DM, Hylton NM, Kuhl CK et al (2003) MRI breast imaging reporting and data system atlas, 1st edn. American College of Radiology, Reston
12. Malich A, Fischer DR, Wurdinger S et al (2005) Potential MRI interpretation model: differentiation of benign from malignant breast masses. AJR Am J Roentgenol 185:964–970
13. Mountford C, Ramadan S, Stanwell P et al (2009) Proton MRS of the breast in the clinical setting. NMR Biomed 22:54–64
14. Schnall MD, Blume J, Bluemke DA et al (2006) Diagnostic architectural and dynamic features at breast MR imaging: multicenter study. Radiology 238:42–53
15. Tsushima Y, Takahashi-Taketomi A, Endo K (2009) Magnetic resonance (MR) differential diagnosis of breast tumors using apparent diffusion coefficient (ADC) on 1.5-T. J Magn Reson Imaging 30:249–255
16. Baltzer PA, Benndorf M, Dietzel M et al (2009) Sensitivity and specificity of unenhanced MR mammography (DWI combined with T2-weighted TSE imaging, ueMRM) for the differentiation of mass lesions. Eur Radiol 20:1101–1110
17. Baltzer PA, Dietzel M, Vag T et al (2009) Diffusion weighted imaging - useful in all kinds of lesions? A systematic review. Eur Radiol 19:765–769
18. Baltzer PA, Renz DM, Herrmann KH et al (2009) Diffusion-weighted imaging (DWI) in MR mammography (MRM): clinical comparison of echo planar imaging (EPI) and half-Fourier single-shot turbo spin echo (HASTE) diffusion techniques. Eur Radiol 19:1612–1620
19. Guo Y, Cai YQ, Cai ZL et al (2002) Differentiation of clinically benign and malignant breast lesions using diffusion-weighted imaging. J Magn Reson Imaging 16:172–178
20. Hatakenaka M, Soeda H, Yabuuchi H et al (2008) Apparent diffusion coefficients of breast tumors: clinical application. Magn Reson Med Sci 7:23–29
21. Kinoshita T, Yashiro N, Ihara N et al (2002) Diffusion-weighted half-Fourier single-shot turbo spin echo imaging in breast tumors: differentiation of invasive ductal carcinoma from fibroadenoma. J Comput Assist Tomogr 26:1042–1046
22. Kuroki Y, Nasu K, Kuroki S et al (2004) Diffusion-weighted imaging of breast cancer with the sensitivity encoding technique: analysis of the apparent diffusion coefficient value. Magn Reson Med Sci 3:79–85
23. Kuroki-Suzuki S, Kuroki Y, Nasu K et al (2007) Detecting breast cancer with non-contrast MR imaging: combining diffusion-weighted and STIR imaging. Magn Reson Med Sci 6:21–27
24. Marini C, Iacconi C, Giannelli M et al (2007) Quantitative diffusion-weighted MR imaging in the differential diagnosis of breast lesion. Eur Radiol 17:2646–2655
25. Park MJ, Cha ES, Kang BJ et al (2007) The role of diffusion-weighted imaging and the apparent diffusion coefficient (ADC) values for breast tumors. Korean J Radiol 8:390–396
26. Rubesova E, Grell AS, De Maertelaer V et al (2006) Quantitative diffusion imaging in breast cancer: a clinical prospective study. J Magn Reson Imaging 24:319–324

27. Wenkel E, Geppert C, Schulz-Wendtland R et al (2007) Diffusion weighted imaging in breast MRI: comparison of two different pulse sequences. Acad Radiol 14:1077–1083

28. Woodhams R, Kakita S, Hata H et al (2009) Diffusion-weighted imaging of mucinous carcinoma of the breast: evaluation of apparent diffusion coefficient and signal intensity in correlation with histologic findings. AJR Am J Roentgenol 193:260–266

29. Woodhams R, Matsunaga K, Iwabuchi K et al (2005) Diffusion-weighted imaging of malignant breast tumors: the usefulness of apparent diffusion coefficient (ADC) value and ADC map for the detection of malignant breast tumors and evaluation of cancer extension. J Comput Assist Tomogr 29:644–649

30. Woodhams R, Matsunaga K, Kan S et al (2005) ADC mapping of benign and malignant breast tumors. Magn Reson Med Sci 4:35–42

31. Charles-Edwards EM, deSouza NM (2006) Diffusion-weighted magnetic resonance imaging and its application to cancer. Cancer Imaging 6:135–143

32. Hagmann P, Jonasson L, Maeder P et al (2006) Understanding diffusion MR imaging techniques: from scalar diffusion-weighted imaging to diffusion tensor imaging and beyond. Radiographics 26(Suppl 1):S205–S223

33. Partridge SC, Murthy RS, Ziadloo A et al (2010) Diffusion tensor magnetic resonance imaging of the normal breast. Magn Reson Imaging 28:320–328

34. Partridge SC, Ziadloo A, Murthy R et al (2010) Diffusion tensor MRI: preliminary anisotropy measures and mapping of breast tumors. J Magn Reson Imaging 31:339–347